Numerical investigation of a spark ignition engine turbulent flow

Numerical investigation of a spark ignition engine turbulent flow

J.A.Beauquel[1]
M.Phil, Loughborough University, LE11 3TU, UK

S.S.Ibrahim[2]
Senior Lecturer, Loughborough University, LE11 3TU, UK

and

R.Chen[3]
Professor, Loughborough University, LE11 3TU, UK

Numerical calculations have been carried out to investigate the transient flow structure inside a four valves, 1.8L Lotus cylinder at an engine speed of 1500rpm. A dynamic mesh CFD simulation has been conducted to represent the real movement of the piston and valves. The main advantage of the dynamic mesh modelling is that it provides the time history of individual flow realisations. Calculations included the inlet port and moving valves so that the flow field can be analysed in detail. The eddy viscosity k-ε RNG turbulence model was used throughout this study. The predicted results were validated against experimental LDA measurements. In this experiment, only air is inserted through the ports into an optically accessible cylinder. Velocity measurements were obtained at different crank-angles and cutting-planes for a standard spark ignition settings and valve lift. The maximum inlet valve lift is 8.5mm with a valve duration of 278º. The maximum exhaust valve lift is 8mm with a duration of 272º. The inlet valves open (IVO), inlet valves close (IVC), exhaust valves open (EVO) and exhaust valves close (EVC) occured at -29º, 249º, 490º and 762º respectively. The volume compression ratio is 10.5. The engine bore is 80.5mm, the stroke is 88.2mm with a connecting rod length of 131mm. In this paper, results are presented and discussed for the variation of turbulence parameters such as turbulence intensity, kinetic energy and its dissipation rate during the intake and compression strokes at various crank-angle positions. The calculation results are in good agreement with the LDA measurements. Moreover, the results have revealed the formation of a strong tumble flow motion during the inlet stroke as well as the creation of a clockwise vortex at the bottom of the cylinder.

Nomenclature

ε	=	turbulent dissipation rate (TDR)
K	=	turbulence kinetic energy (TKE)
ρ	=	density
μ	=	dynamic viscosity

I. Introduction

Although the experimental studies on flow inside internal combustion (IC) engines using the laser Doppler anemometry (LDA) and particle tracking velocimetry (PTV) can provide a physical insight into the real flows inside the cylinder (Li *et al*., 2001; Gasparetti *et al*., 1996), the use of such experimental technology is usually expensive and it is still impossible for obtaining the entire flow details for IC engines in practice.

As an alternative, the use of computational aided design (CAD) and computational fluid dynamics (CFD) has become popular in optimisation design of IC engines. However, the results of CFD modelling have to be

[1] PhD student, Aeronautical and Automotive Engineering Department, Loughborough University, Leicestershire, LE11 3TU, UK / j.a.beauquel@lboro.ac.uk
[2] Senior lecturer, Aeronautical and Automotive Engineering Department, Loughborough University, Leicestershire, LE11 3TU, UK / s.s.ibrahim@lboro.ac.uk
[3] Professor, Aeronautical and Automotive Engineering Department, Loughborough University, Leicestershire, LE11 3TU, UK / r.chen@lboro.ac.uk

validated against relevant experiments. One of the advantages of CFD modelling is that the settings for simulation can be recorded and these will provide basis for further studies. CFD modelling of turbulent flows inside combustion chamber of vehicle engines have been used for many years (Mao *et al*., 1994; Affes *et al*., 1998; Chen and Shih, 1997; Gharakhani and Ghoniem, 1997; Isshiki *et al*., 1985; Lebrere *et al*., 1996; Pierson and Richardson, 1999; Zhu, 1995).

Due to computer restriction, it seems that several previous studies of CFD modelling on IC engines either introduced simplifications to ease the 3D geometry of the cylinder, or imposed some idealised boundary conditions/motions in the calculations. For instance, the use of rectangular prisms (stairsteps) simplifies the mesh (Isshiki *et al*., 1985) or steady flow studies inside the cylinder reduce the computational time (Isshiki *et al*., 1985; Lebrere *et al*., 1996; Chen and Shih, 1997; Arcoumanis *et al*., 1988). Constant valve lift is another factor that can reduce the difficulty of modelling engine flow (Gharakhani and Ghoniem, 1997; Chen and Shih, 1997). Arcoumanis *et al*. (1988), Aita *et al*. (1991), Gosman *et al*. (1984) and Wakisaka *et al*. (1986) considered the valves as a single moving plate; for the latter, the modelled flow field was found to be very different from the experimental results, as a consequence of such simplification.

Recent increase of computing capabilities allows studies of full cycle engine simulation with moving valves (Zhu, 1995; Pierson and Richardson, 1999; Affes *et al*., 1998). The k-ε model is used in most of those studies and usually shows good agreement with experimental comparisons (Zur Loye *et al*., 1989; Kono *et al*., 1991; Chen *et al*., 1998; Yavuz and Celik, 1999). The studies usually depict in-cylinder tumble and swirl. For the case of Li *et al*. (2001), the CFD modelling results clearly showed that there exist two counter rotating vortices in the cylinder.

It is the aim of this paper to present results of a CFD study of transient flow characteristics inside the cylinder during the intake stroke. The predicted results are validated against experimental LDA measurements as reported by Pitcher et al. (2003).The results obtained in terms of mean velocities and velocity vectors are presented. Three-dimensional calculations of the intake stroke have been carried out for a 1.8L Lotus engine cylinder at an engine speed of 1500rpm. No simplifications of the geometry are made and the intake calculations include the inlet port and moving valves so that the flow field can be analysed in detail. The mean velocities are compared with LDA measurements for a model validation. Hence, the evolution of the flow pattern inside the cylinder, the turbulence kinetic energy, the turbulent dissipation rate and the turbulence intensity can be described for the symmetrical cross section.

II. Model Development

A. Dynamic Mesh of Inlet Valve and Piston Movements

In this study, the camshaft profile is given for every 2 crank angle degrees (CAD) of the engine cycle. Thus, a valve position text file is created to be inserted as a profile into the calculations. The inlet valves lift has a maximum of 8.5mm at 100º and the exhaust valves lift has a maximum of 8mm at 616º. Another important aspect of dynamic modelling is the piston displacement. The crankshaft rotates around its axis and its motion is defined by the crank angle relative to this axis. During the inlet stroke, the piston is pulled by the connecting rod and it moves downward linearly from Top Dead Centre (TDC) to Bottom Dead Centre (BDC). In the meantime, the two inlet valves are opened and the exhaust valves remain closed. The dynamic mesh type needs to be selected depending on each part of the geometry. For this study, the upper part of the cylinder including the inlet ports is meshed using tetrahedrons and pyramids. The cells directly in contact with the valves stems are meshed using hexahedrons and prisms which allow the layering option to be activated. This enables the valves movements. The local remeshing is set to remesh the cells around the valves for every step to avoid cell distortion. Also, the lower part of the cylinder is meshed using hexahedrons and prisms. The software will simulate the piston motion by creating layers of cells. Since different mesh types are adopted for the upper and lower portions of the cylinder, the two mesh systems have to be matched.

The boundary condition imposed on the inlet port is pressure-inlet and the piston and the valves are defined as moving walls. The valves are defined and matched to the velocity profile to be updated for each crank angle degree. The convergence criteria for velocity and continuity are set to 10^{-4}. For the convergence criteria discussed, the simulation usually takes 70-80 iterations to converge. Thus the maximum number of iterations is specified as 200, allowing the simulation to converge far before the maximum number of iterations is reached. Specification of a maximum number of 200 iterations hence avoids the simulation running endlessly whilst achieving a satisfactory compromise for model accuracy. The numerical details for this particular geometry and engine speed can be calculated. The measured piston stroke is 88.2 mm. Hence, the average piston speed is 4.41m/s at 1500rpm. The operating pressure is assumed to be 101,325Pa. The density at 300ºK is set at ρ = 1.225kg/m³ and the dynamic viscosity $\mu = 1.79\times10^{-5}$kg/ms. With an hydraulic diameter value of 0.0385m, it is found that the flow through the whole cylinder will be turbulent.

B. Engine Parameters

The engine experimental data used for model validation are based on Laser Doppler Anemometry (LDA) measurements conducted by Pitcher *et al.*, 2003. In this engine test rig, only air is inserted trough the ports into an optically accessible cylinder. Laser beams measure the velocity vectors of various points in the cylinder for two dimensions at different crank-angles and cutting-planes. These experimental data were obtained for standard spark ignition settings and valve lift at an engine speed of 1500rpm. The maximum inlet valve lift is 8.5mm with valve duration of 278º; the maximum exhaust valve lift is 8mm with a lift duration of 272º. The inlet valves open (IVO), inlet valves close (IVC), exhaust valves open (EVO) and exhaust valves close (EVC) occur at -29º, 249º, 490º and 762º respectively. The 4 valves engine volume is 1.8L with a compression ratio of 10.5:1. The engine bore is 80.5mm, the stroke is 88.2mm with a connecting rod length of 131mm. The laser beams are set to measure velocity vectors on three different planes. Due to experimental limitations, the laser beams are set to measure velocity vectors on only three different planes, namely A, B and C plans. The A plane is the cross-plane cutting inlet and outlet ports at Y=0mm; the B plane is the centre-plane of the cylinder at X=0mm and the C plane is the cross-plane cutting inlet and outlet ports 18 mm from the centreline at Y=-18mm. The points defined on the A, B and C planes to measure velocity vectors are defined by six lines on the Z axis from -10mm to -60mm every 10mm (-10, -20, -30, -40, -50, -60), 0mm being TDC. Points are defined on those lines every 5mm, from -35 to 35mm on the A plane and B plane, from -30 to 30mm on the C plane due to a smaller cross-section. It should be noted that the 0mm values were not recorded during the experiments. For the A and B planes, measurements are made on 6 lines, recording 14 points for each line, which gives a total of 84 points per plane. As the C plane is 18mm from the centreline, the cross-section is smaller and only 12 points are recorded from -30 to 30mm. This gives a total of 72 values for the C plane. Two velocity components respective to their planes are recorded separately for each of these points by the laser beams every 4º for the cycle of 720º.

III. Results

The simulations are set to match a step size of 1CAD when possible and 0.5CAD when a moving part is included. If the full cycle of 720º is calculated with a step angle size of 0.5º, the simulations take 1440 steps per cycle to complete. However, during dynamic movement of the piston and valves for CFD simulations, computational crashes may happen depending on the geometry. Those crashes can be of different kind: excessive temperature or pressure limit, negative cell creation even in only one cell in the whole geometry. One way to avoid computational error is to reduce the step angle size up to 0.05º when needed. Hence, the dynamic movement is reduced between two steps which will limit the variation of the temperature, pressure and cell variation in the model. Also, depending on the engine cycle number, crashes may occur at different crank-angles. The strategy to save computational time is to deactivate the inlet and exhaust ports when their respective valves are closed. When the ports are deactivated, the number of cells totalled 79,356 at TDC and 244,222 at BDC. The inlet and exhaust valves have only lift duration of 278º. With a safe port activation margin of 1º before and after the valve movements, it means that each port (inlet and exhaust) can be deactivated for 440º over the cycle of 720º. Two sets of CFD calculation demonstrated that the activation and deactivation of inlet and exhaust ports are not affecting the results. According to those CFD calculations, this method can save approximately 40% of the computational time. The port events are defined into the computational solutions and could be summarised as follow:

- Inlet and exhaust ports activated from 0 to 44CAD
- Inlet port activated and exhaust port deactivated from 44 to 250CAD
- Inlet and exhaust ports deactivated from 250 to 488CAD
- Exhaust port activated and inlet port deactivated from 488 to 690CAD
- Inlet and exhaust ports activated from 690 to 720CAD

To validate the numerical solution against experimental results, different simulations are set to investigate the possible variations of mean velocity, vorticity, turbulent kinetic energy and cylinder pressure due to the following variables:

- Crank-angle step size during the cycle
- Deactivation and activation of the exhaust and inlet ports
- Maximum numbers of iteration for residuals
- The variation of velocity between cycles
- Air models
- Turbulence model used
- Computational grid resolution

It is found that the crank-angle step size can be varied during the cycle to avoid crashes and reduce the computational time without affecting the results. Also, the inlet and exhaust ports can be activated and de-activated during the cycle to reduce simulation time by 40% without altering the cylinder pressure. Calculations

with different maximum number of iteration and residuals are conducted to quantify the pressure variation if the convergence criteria are not reached. The results show that 200 maximum iterations per step allow reducing the time of calculation while keeping a good compromise for accuracy. An additional study is conducted to assess the computational cycle-to-cycle variation. Starting from cycle one, five cycles are calculated which demonstrates a consequent difference in terms of mean velocity levels. The first stable cycle found to be the third one, thereafter all the cycles demonstrate the same level of mean velocity. An air density study shows that the ideal gas model is found to perform better and shows good agreement with the experimental data. When testing three different turbulence models, the k-ε RNG (Yakhot and Orszag, 1986) model demonstrates the best results and will therefore be used for the rest of the study. Finally, a grid dependency is conducted to determine the best compromise for mesh size. The facet average vorticity and turbulent kinetic energy are compared for the three different grids of 3mm, 2mm and 1.5mm. As a result, the medium grid can be used to reduce the computational time without compromising the results. For this grid, the mesh quality can be studied. The number of cells totalled 154,546 at TDC. When the mesh quality is characterised by the equisize skew, the statistics showed that 92,890 cells have a factor of 0-0.4. Again, when the mesh quality is characterised by the equiangle skew, the statistics show that 85,448 cells have a factor of 0-0.4. This indicated that 60.11% of the mesh cells are high quality when judging by the equisize skew and 55.29% of the cells are high quality if they are judged by the equiangle skew. The cell number increases gradually until the piston reaches BDC. It is indicated from the simulation that the total number of cells reaches 319,412 at BDC. It is found that the mesh cell creation from TDC to BDC is improving the overall mesh quality for both equisize and equiangle skew by over 20%.

IV. Validation

A comparison between experimental and numerical results can be drawn for model validation as shown in figure 1. The computational results total 2137 values in time during the intake stroke and compression stroke for each of the 84, 84, 72 measurement points for the three planes A, B, C respectively. Those values are reported on graphs for an easier comparison between CFD and LDA results. Due to the amount of data, only results from plane A are presented in this paper. The rest of the results are regrouped and summarised to describe the accuracy of the CFD model for all points of plane A, B and C. On the A plane, only two lines of six points will be represented in figures. On each side of the cylinder, the points are separated 30mm from the centreline as shown in Figure 2. The axial mean velocities of those points are represented in figure 1 for both the experimental and calculated values.

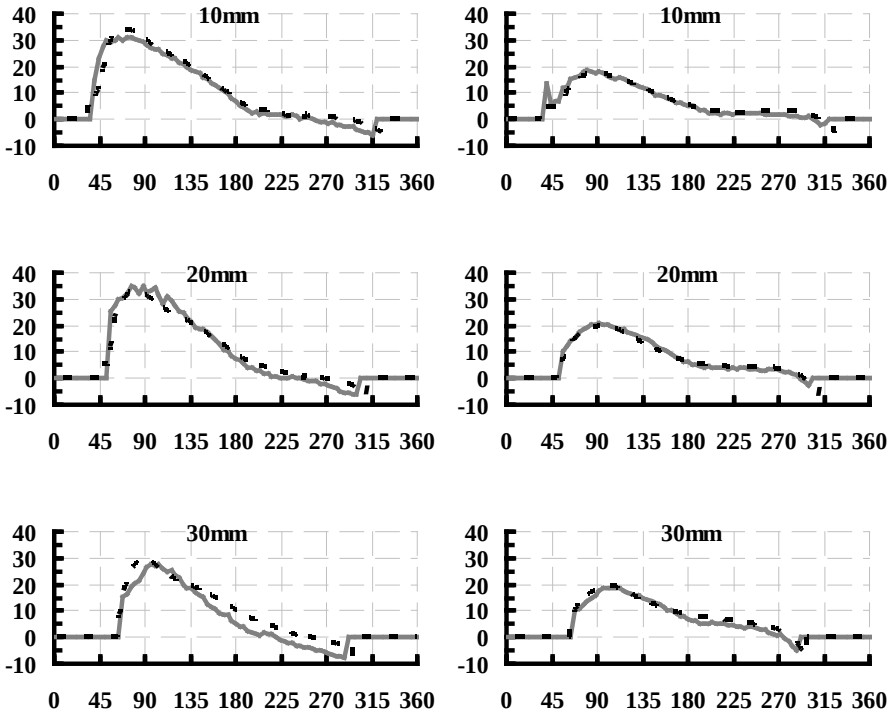

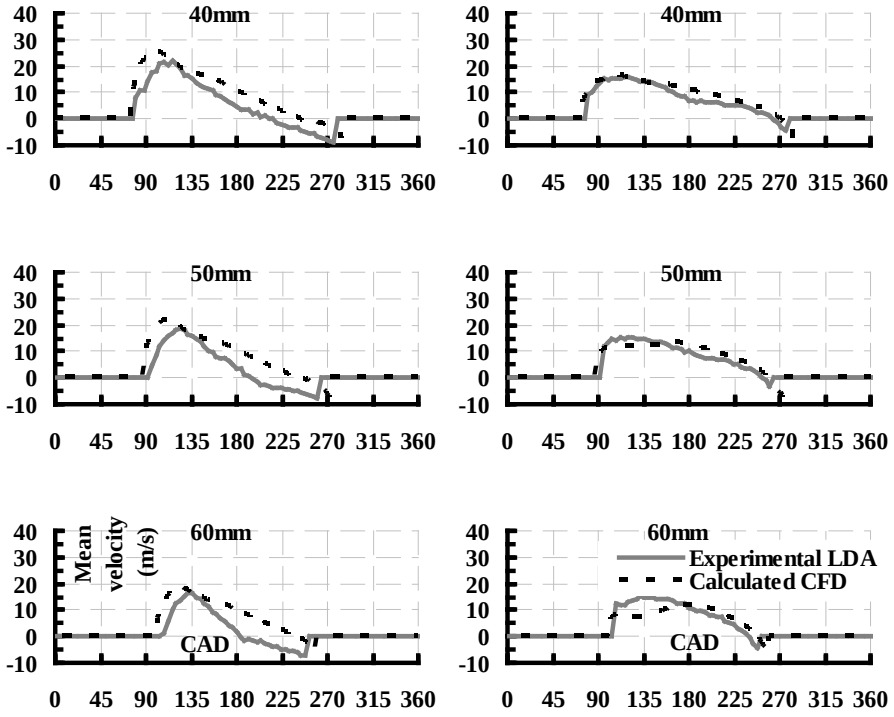

Figure 1. Axial mean velocity on the -30mm (left) and +30mm radial line (right) for 10mm, 20mm, 30mm,40mm, 50mm and 60mm axial lines

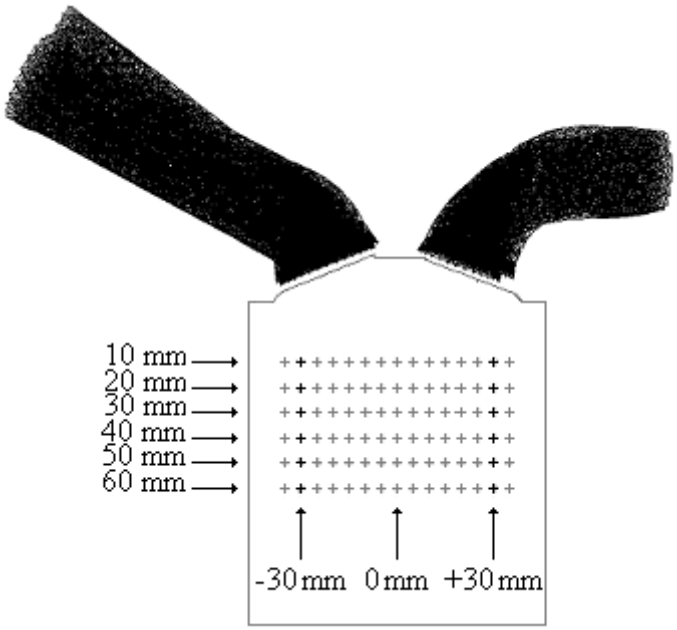

Figure 2. Selected points on the A plane

Observing the results for both CFD and LDA, it can be concluded that:

- The CFD calculations are in good agreement with the LDA in particular for the positive radial line of points.
- The top half of the cylinder is demonstrating nearly matching results
- The positive radial part of the cylinder is showing more accurate results than the negative part
- The CFD results show an over-prediction of the negative radial line of points. This is particularly true for the bottom half of the cylinder.

A total of 240 measurement points are distributed on the three planes. Each point of each plane has 2137 time dependent mean velocities obtained with numerical calculation for the intake and the compression strokes. Each velocity point obtained

by LDA measurement has 90 values in time for 360CAD, one every 4º. All the velocity results, CFD and LDA, contain separated values for radial and axial values. This gives an excessive amount of data collected. Therefore, an average result is necessary to describe the overall performance of the model. In order to define how the numerical model predicts the flow patterns inside the whole cylinder, each point of the specific plane can be averaged for its own value in time. From 40CAD to 280CAD, the overall correlation of the model is found to be 78.32%.

The CFD results obtained can be used to describe the evolution of the intake flow pattern inside the cylinder using velocity vectors. Two typical crankshaft angles of 90º and 180º are selected to characterise the flow field evolution inside the cylinder, which corresponds to the second half of the intake stroke. At these angle values, the corresponding displacement of the inlet valves is 8.41mm and 3.12mm for 90º and 180º, respectively. It should be noted here that the maximum inlet valve lift of 8.5mm occurs at a crankshaft angle of 100º, corresponding to a piston displacement of 59.17mm. Figure 3 shows the velocity field evolution in inlet port symmetry plane for two crankshaft angles. At a crankshaft angle of 90º, the tumble motion is just formed as can be seen from Figure 3a. The highest velocity of the flow occurs at the region marked as "①"at approximately 40m/s. It can be seen that the main part of the high velocity flow is at the top of the cylinder and around the valves. The flow diverges around the valve to generate two counter rotating tumble vortices "②" and "③". Such counter rotating flow is deflected by the cylinder wall and piston, resulting in the loss in intensity of the vortices. It can be seen that the clockwise tumble vortex "②" is stronger than "③" at this stage. The vortices rotational centre is marked as "④". At this angle, the piston velocity is 6.95m/s and the openness of the valve is 98.94% of the maximum valve lift. The maximum velocity found from the simulation in the symmetry plane is 7.31m/s at 74CAD. Since the valves are nearly fully opened at this angle, the incoming flow can easily enter the cylinder with less valve obstruction. This velocity difference can be expressed as a factor between the piston area and the inlet wetted area. The bore is equal to 0.0805m which gives a piston area of $5.09 \times 10^{-3} m^2$. The inlet hydraulic diameter of 0.0385m gives a wetted area of 1.16×10^{-3} m². With an instantaneous piston velocity of 6.95m/s, the corresponding multiplying coefficient between the wetted area of the inlet and the piston surface of 4.38 would give a velocity of 30.44m/s at the inlet surface. This can be explained by the additional flow restriction around the valves. It can also be due to a time delay of air flow between the piston and inlet surface. Figure 3b depicts the flow pattern at a crankshaft angle of 180º. At this angle, the piston velocity is nil and the valve lift of 3.12mm represents an openness of 36.7%. Although the flow velocities have reduced as the result of reduction in piston speed when the crankshaft angle is greater than 74º, the overall flow inside the cylinder is strongly affected by the inertia of the tumble motion. The flow at "①" still diverges around the valve to generate two counter rotating tumble vortices "②" and "③" as in Figure 3a. The conical jet marked "③"evolves into a larger rotating vortex inside the cylinder. The strength of the vortices has now changed compared to the previous flow behaviour at 90º. The anti-clockwise rotating tumble "③" is reaching a maximum of 15m/s while "②" is attaining 8m/s. However, the turbulence seen as "④" in Figure 3b is slightly moving up in the cylinder. It is noticed that a secondary vortex marked "⑤" is formed at the bottom right-hand side of the cylinder as a result of resultant interaction of flow deflection by the piston, the inertia of the impinging jet and their differences in strength. This clockwise vortex confirms that the rotating tumble vortex "②" is faster than vortex "③". The sizes of the two major tumble vortices increase due to the increase in cylinder volume.

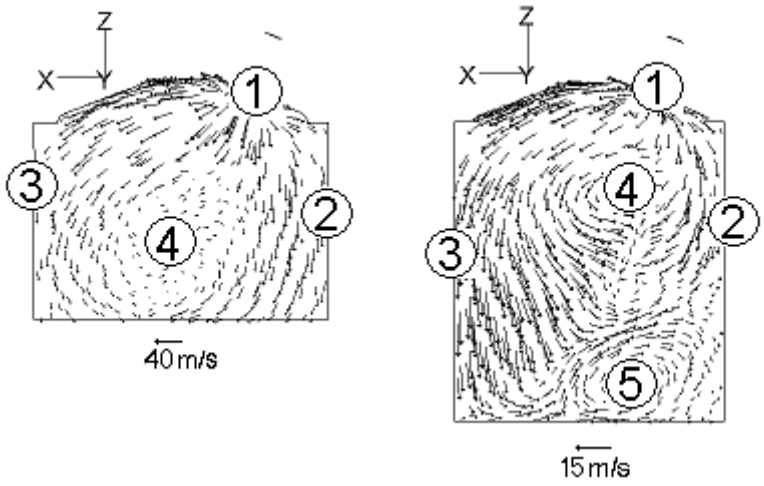

(a) (b)

Figure 3. Velocity magnitude of the A cutting plane at (a) 90 CAD, (b) 180 CAD

Figure 4 represents the line averaged values for different depths into the cylinder (lines 10mm to 60mm). All turbulence figures depict a maximum when the piston reaches the specific line during the inlet stroke. For instance, when the piston passes the 10mm line at 35CAD, the turbulence intensity (TI), the turbulence kinetic energy (TKE) and the turbulent dissipation rate (TDR) are already at 1.8%, $6.5 m^2/s^2$ and $24{,}000 m^2/s^3$ respectively. AT 35CAD, the inlet valves are already opened. It can be clearly seen that the turbulences increase progressively until the maximum valve lift at 100CAD. For the line 10mm, the level of TI, TKE and TDR reaches a maximum value of 3.8%, $25 m^2/s^2$ and $45600 m^2/s^3$ at 84CAD, 82.5CAD and 80CAD respectively. The peak of turbulence seen on the 10mm line can be explained by the proximity with the inlet valves. The flow being directed by the valves to form the tumble and swirl phenomena is stronger on the 10mm line. As a

result, the maximum turbulence intensity found on lines 20mm to 60mm is decreasing to 3.5% at 112CAD, 3.3% at 130CAD, 3.15% at 138CAD, 3.1% at 149CAD and 2.95% at 161CAD, respectively. Same tendencies for the maximum values are observed for TKE and TDR. This confirms the phenomena of air inertia as the mixture is entering the combustion chamber. The turbulences created by the valves shape are distributed inside the combustion chamber during the intake stroke. At the end of the intake stroke, the piston speed reduces and the turbulences decrease for all lines inside the cylinder. This is also related to the high dissipation rate seen during the intake stroke. As the piston is moving up and picking up speed during the compression stroke, the line 60mm to 10mm see their turbulence intensity rising again. As the inlet valves are now closed since 249CAD, only the piston movement is affecting the turbulences which explains lower levels compared to the intake stroke. On this particular symmetry plane, the turbulence intensity on the 10mm line has varied between 2% and 3.8% to finish around 3.1% at 326CAD. The high turbulence intensity and turbulent kinetic energy during the intake and compression stroke are necessary for mixing the air with the fuel while they will directly affect the flame propagation at the end of the compression stroke.

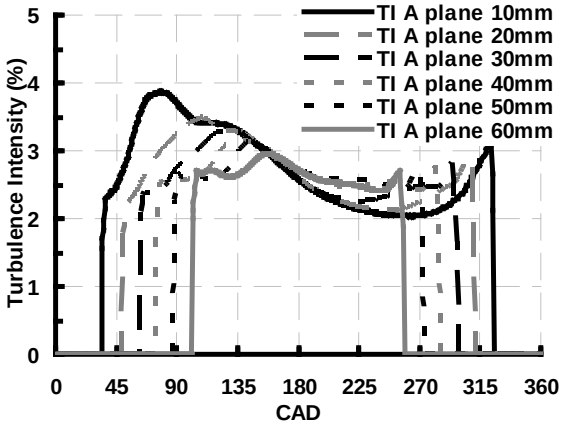

(a)

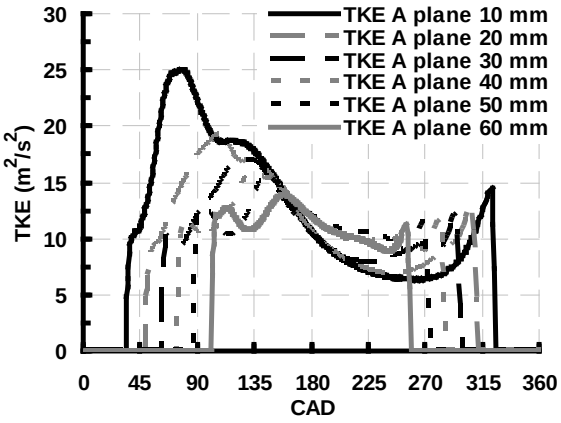

(b)

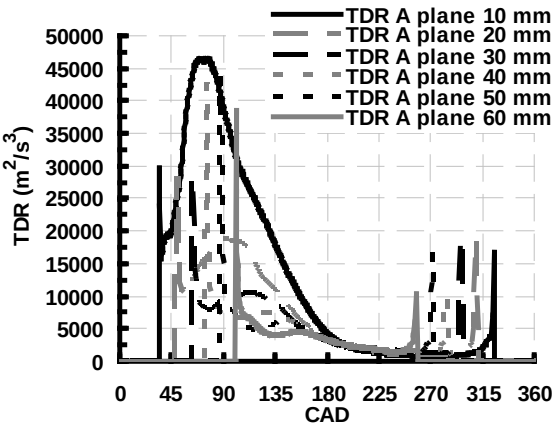

(c)

Figure 4. Line average turbulence intensity (a), turbulence kinetic energy (b) and turbulent dissipation rate (c) for the A cutting plane

V. Conclusion

In most of the previous studies of CFD modelling of the flow inside a cylinder, the simulations are usually conducted by fixing the positions of piston and valves. Such simulations can only deliver a limited physical insight into the flow inside the cylinder. In the present study, a dynamic mesh CFD simulation of transient flow inside an internal combustion engine cylinder during the intake stroke has been conducted using the real movement of the piston and valves. The first part intends to validate the model with a comparison between experimental and simulated data. It is found that the calculations are in good agreement with the LDA measurements in particular for the positive radial line of points and top half of the cylinder. Over-prediction is noticed for the negative radial lines of points at the bottom half of the cylinder. However, the overall averaged prediction of the CFD model is found to be 78.32% from 40CAD to 280CAD. The second part of the study describes the evolution of the flow pattern and turbulence levels inside the cylinder at the symmetrical cross section. The conclusions drawn from this study are summarised as follows:

(1) One of interesting aspects of the dynamic mesh modelling is that the modelling provides the time history of individual flow realisations. The simulation of the transient flow inside the cylinder has clearly revealed the existence of tumble phenomenon for the inlet stroke. This has been reported previously by experimental studies in this area of research. Tumble motion was developed significantly during the intake stroke.

(2) As the movements of the valves and piston are modelled, vortex centres change inside the cylinder. The tumble centre is moving up slightly from 90CAD to 180CAD. The predicted flow behaviour shows the creation of a clockwise vortex at the bottom of the cylinder.

(3) The simulations show that when the engine runs at a rotational speed of 1500rpm, the effect of inertia of air is significant, which develops an air flow delay.

(4) The variation of turbulence levels such as turbulence intensity, turbulent kinetic energy and turbulent dissipation rate have been drawn for the intake and compression strokes. Their variations will induce the mixing of air and fuel during intake and compression strokes while high levels of turbulence will directly affect the flame propagation at the end of the compression stroke.

(5) The LDA experimental data has proven necessary to validate the numerical results for the mean velocity which can later lead to flow behaviour description especially for the tumble motion. However it seems that an improvement can be made by recording experimental data every 1CAD instead of 4CAD to increase the accuracy of the comparison. Also, additional data as radial cross section would be needed to validate the swirl motion.

References

Journal papers

[1]Li, Y., Liu, S., Shi, S.X., Feng, M. and Sui, X., 2001, An investigation of in-cylinder tumbling motion in a four-valve spark ignition engine, *Proceedings of the Institution of Mechanical Engineering*, **215**, 273-284.

[2]Gasparetti, M., Paone, N. and Tomasini, E.P., 1996, Laser Doppler techniques for the combined measurement of inlet flow and valve motion in IC engines, *Measurement Science and Technology*, **7**, 576-591.

[3]Mao, Y., Buffat, M. and Jeandel, D., 1994, Simulation of the turbulent flow inside the combustion chamber of a reciprocating engine with a finite element method, *Journal of Fluid Engineering*, **116**, 37-46.

[4]Affes, H., Chu, D. and Smith, D.E., 1998, The application of shape optimization techniques to automotive engine fluid flow problems, *ASME Fluids Engineering Division Summer Meeting*, Paper No.98-4845, 1-8.

[5]Chen, Y.S. and Shih, M.H., 1997, CFD applications to internal combustion engine port-flow designs, *ASME Fluids Engineering Division Summer Meeting*, Paper No.97-3024, 1-8.

[6]Gharakhani, A. and Ghoniem, A.F., 1997, Toward a grid-free simulation of the flow in engines, *ASME Fluids Engineering Division Summer Meeting*, Paper No.97-3025, 1-9.

[7]Isshiki, Y., Shimamoto, Y. and Wakisaka, T., 1985, Numerical prediction of effect of intake port configurations on the induction swirl intensity by 3-dimensional gas flow analysis, *Comodia*, 295-304.

[8]Lebrere, L., Buffat, M., Le Penven, L. and Dillies, B., 1996, Application of Reynolds stress modeling to engine flow calculations, *ASME Journal of Fluids Engineering*, **118**, 710-721.

[9]Pierson, S. and Richardson, S., 1999, Computer simulation of the inlet port helps improve fuel economy and emissions, *Fluent Journal*, Paper No.JA095, 1-3.

[10]Zur Loye, A.O., Siebers, D.L., Mckinley, T.L., Ng, H.K. and Primus, R.J., 1989, Cycle-resolved LDV measurements in a motored diesel engine and comparison with k-ε model predictions, *Society of Automotive Engineers*, Paper No.890618, 1-17.

[11]Arcoumanis, C., Hadjiapostolou, A. and Whitelaw, J.H., 1988, Swirl center precession in engine flows, *Society of Automotive Engineers*, Paper No.870370, **4**, 365-379.

[12]Aita, S., Tabbal, A., Munck, G., Montmayeur, Y. and Aoyagi, Y., 1991, Numerical simulation of swirling port-valve-cylinder flow in Diesel engine, Paper No.910263, 1-12.

[13]Gosman, A. D., Tsui, Y. Y. and Watkins, A. P. 1984, Calculation of three dimensional air motion in model engines, *Society of Automotive Engineers*, Paper No.840229, **2**, 56-84.
[14]Wakisaka, T., Shimamoto, Y. and Issihiki, Y., 1986, Three-dimensional numerical analysis of in-cylinder flows in reciprocating engines, *Society of Automotive Engineers*, Paper No.860464, 1-18.
[15]Zhu, T.T., 1995, Explosive results: simulating a 4-stroke engine cycle, *IEEE Computational Science and Engineering*, **2**, 4-5.
[16]Kono, S., Terashita, T. and Kudo, H., 1991, Study of the swirl effects on spray formations in DI engines by 3D numerical calculations, *Society of Automotive Engineers*, Paper No.910264, 1-10.
[17]Chen, A., Veshagh, A. and Wallace, S. 1998, Intake flow predictions of a transparent DI Diesel engine, *Society of Automotive Engineers*, Paper No.981020, p147-159.
[18]Yavuz, I. and Celik, I., 1999, Applicability of the k-epsilon model for IC-engine simulations, *ASME/JSME Joint Fluids Engineering Conference*, Paper No.99-7318, 1-6.
[19]Pitcher, G., Turner, J., Wigley, G. and Chen, R., 2003, A comparison of the in-cylinder flow fields generated for spark and controlled auto-ignition, *Proceedings of the SAE Fuel & Lubricant Meeting*, Paper No.2003-01-1798, 1-7.
[20]Yakhot, V. and Orszag, S. A., 1986, Renormalization Group Analysis of Turbulence: I. Basic Theory, *Journal of Scientific Computing*, 1(1):1-51.